Biochimica et Biophysica Acta 1828 (2013) 1918–1925

Contents lists available at SciVerse ScienceDirect

Biochimica et Biophysica Acta

journal homepage: www.elsevier.com/locate/bbamem

Vesicle deposition and subsequent membrane–melittin interactions on different substrates: A QCM-D experiment

Nai-Yan Lu [a], Kai Yang [b], Jing-Liang Li [c], Bing Yuan [b,*], Yu-Qiang Ma [a,b,**]

[a] National Laboratory of Solid State Microstructures and Department of Physics, Nanjing University, Nanjing, 210093, PR China
[b] Center for Soft Condensed Matter Physics and Interdisciplinary Research, Soochow University, Suzhou, 215006, PR China
[c] Centre for Material and Fiber Innovation, Deakin University, Waurn Ponds, Vic 3216, Australia

ARTICLE INFO

Article history:
Received 11 December 2012
Received in revised form 21 February 2013
Accepted 12 April 2013
Available online 20 April 2013

Keywords:
QCM-D
Lipid membrane
Melittin
Different substrate

ABSTRACT

Quartz crystal microbalance with dissipation (QCM-D) technique is one of the most effective methods to monitor the dynamic behaviors of a layer on a solid surface. Moreover, it has been reported recently that it is able to provide a fingerprint for the peptide–membrane interactions. In this work, QCM-D technique combined with computer simulations was employed to investigate the deposition and transformation of vesicles, as well as the subsequent membrane–melittin interactions on different substrates. A range of substrate surfaces, i.e. naked SiO_2 without or with Au/polyelectrolyte coating, were produced. The nature of the substrate determined whether the adsorbed vesicles were present as a high-quality supported bilayer or an assembled vesicle matrix, which consequently influenced the membrane–melittin interactions. It was indicated by the related computer simulations that the lipid packing state of the membrane was a key factor to determine the mechanism of membrane–peptide interactions. Furthermore, this work might be a good example of the application of QCM-D for the exploration of membrane-active peptides.

1. Introduction

Supported lipid bilayers (SLBs) serve as models of cellular membranes and provide a controlled environment for characterizing membrane-related interactions [1–3]. The preparation of SLBs has attracted great interest for both fundamental research [4,5] and applications such as in molecular biology and biotechnologies [6,7]. One of the advantages of SLBs is that they lie flat on a surface, making them compatible with various surface-sensitive analysis techniques such as atomic force microscopy (AFM) and dissipative quartz crystal microbalance (QCM-D). A common way to fabricate SLBs is vesicle fusion *via* vesicle adsorption followed by spontaneous rupture of the adsorbed vesicles to form a confluent lipid membrane. A major disadvantage of such method is that an incomplete vesicle fusion may be resulted, leading to the presence of residual vesicles on the surface. The remaining vesicles inevitably disturb the characteristic behaviors of a SLB. A variety of strategies, such as substrate surface modification [8,9], polymer cushion [10,11] and peptide addition [12], have been explored to study, modulate, and/or improve the SLB formation process. Generally, three types of interactions, namely substrate surface-vesicle interaction, intervesicle interaction, and intravesicle molecular interaction, are regarded as key factors influencing the deposition pathway of vesicles on a substrate [13].

The biological activity of antimicrobial peptides (AMP) has been extensively studied for their potential applications as food preservatives, antiseptic agents and alternatives for conventional antibiotics [14–18]. Melittin is a typical model for the investigations of AMP [19]. The biological activity of melittin has been studied on both whole bacterial cells [16,20] and model membranes [21,22] with many biophysical techniques including surface plasmon resonance (SPR) [23], fluorescence anisotropy measurements [17], atomic force microscopy (AFM) [13], and QCM-D [24]. In the membrane environment, melittin folds into amphiphilic α-helices with four positive charges located at the C-terminus. One widely accepted model believes that melittin at high concentrations can insert into (mostly as toroidal pores) a membrane and destabilize the membrane resulting in leakage of cell components and eventually cell death (the "carpet" mechanism) [25,26]. Besides the lipid composition (e.g. charged components [27,28] and cholesterol [29,30]), the morphology such as curvature of the membrane was shown to have an important impact on the membrane affinity of melittin [31]. However, questions concerning the exact mechanism have not been fully answered yet.

The QCM-D method is an attractive technique for real time and in situ measurement of the dynamic behaviors of a layer on the crystal surface. It provides information of both the mass and structural changes occurring to the layer [9,32]. Therefore, QCM-D is considered as a powerful tool to study the dynamic processes of adsorption, desorption, and interfacial interactions between a supported membrane

* Corresponding author. Tel./fax: +86 512 65220239.
** Correspondence to: Y-Q. Ma, National Laboratory of Solid State Microstructures and Department of Physics, Nanjing University, Nanjing, 210093, PR China. Tel./fax: +86 25 83592900.
E-mail addresses: yuanbing@suda.edu.cn (B. Yuan), myqiang@nju.edu.cn (Y.-Q. Ma).

0005-2736/$ – see front matter © 2013 Elsevier B.V. All rights reserved.
http://dx.doi.org/10.1016/j.bbamem.2013.04.013

and lipid-active peptides [13,33–35]. In our previous work, we studied the molecular-level interactions of melittin with SLBs by varying the lipid state and the local peptide-to-lipid ratio, with a combination of QCM-D technique and computer simulations [24]. To obtain more insights into this process, we investigated in this work on different substrates, the deposition and deformation of vesicles, and the subsequent dynamic interactions between melittin and the fabricated membrane, i.e. SLB or vesicle matrix. SiO_2, Au, or polyelectrolyte coated substrates were produced in the study. We will show that the substrate determines the SLB formation process. Subsequently, the characteristic properties of a SLB or vesicle matrix significantly affect the membrane–melittin interactions. Results of the present study will help understand the mechanism involved. Furthermore, QCM-D combined with computer simulations is proven effective in studying the dynamic interactions between a peptide and a supported membrane of both SLBs and vesicles.

2. Materials and methods

2.1. Chemicals

1,2-Dioleoyl-*cn*-glycero-3-phosphocholine (DOPC), 1,2-dipalmitoyl-*sn*-glycero-3-phosphocholine (DPPC), and cholesterol (Chol) were purchased from Avanti Lipids (Fig. 1). Buffer solution (10 mM tris(hydroxymethyl)-aminomethane, 100 mM NaCl, and 2 mM $CaCl_2$) was adjusted to pH 7.5 with HCl. Melittin from honey bee venom was obtained from Sigma and dissolved in buffer to 2 μg mL^{-1} (being above the minimum milittin concentration for erythrocyte release of 0.85 μg mL^{-1}, *cf.* Supporting Information) [36].

Poly(diallyl dimethyl ammonium chloride) (PDDA, M_w 100 000) and poly(sodium 4-styrenesulfonate) (PSS, Mw 100 000, 35% aqueous solution) were obtained from Adamas. The polyelectrolytes were used without further purification. Both polyelectrolyte deposition baths were employed as 1 wt.% solutions in distilled water.

2.2. Vesicle preparation

A solution of monodisperse unilamellar lipid vesicles was prepared by a conventional extrusion method as described previously [24]. Lipids at desired ratios (DOPC:DPPC:Chol = 4:4:2) were first dissolved in chloroform, and then dried completely in a N_2 stream. After that they were rehydrated in Tris buffer to 3.5 mg mL^{-1} lipid at 50 °C. The suspensions were extruded 21 times through a 100 nm pore polycarbonate membrane (Avanti Polar Lipids). Light-scattering measurements revealed that vesicles with a typical size of ~110 ± 15 nm were obtained (Figure S1) [8]. The vesicle suspensions were stored at 4 °C and used within 3 days. The vesicles were diluted in a buffer solution to a lipid concentration of 0.07 mg mL^{-1} for use. All the operations were carried out at 25 °C.

2.3. QCM-D monitoring

QCM-D measurements were performed on a Q-sense E1 instrument (Sweden). AT-cut quartz crystals with a fundamental frequency of 5 MHz and a diameter of 14 mm were used. The change of resonance frequency (Δf) and energy dissipation (ΔD) during experiments were monitored simultaneously at six different overtones of the natural frequency (from 3rd to 13th, i.e., 15–65 MHz). Measurements at the natural frequency (5 MHz) were not considered as this resonance is very sensitive to changes of bulk solution which would lead to unreliable information [9]. A flow-through system was employed and maintained throughout the measurement. An Ismatec peristaltic pump (Sweden) was used to control the liquid rate at 50 μL min^{-1}.

Two kinds of top coatings of the sensor crystal, SiO_2 and Au, were utilized as working surfaces in this work. The PE cushion was deposited on the SiO_2 surface by a layer-by-layer method under QCM-D monitoring as specified in Section 4.1. After each measurement, the crystal was taken out from the chamber and cleaned carefully for next use. The SiO_2 surface of the sensor crystal was immersed in a 2 wt.% SDS for 30 min and rinsed with water. However, for the Au surface, the crystal was further incubated in a 75 °C ammonium-peroxide solution (ammonia: hydrogen peroxide:water = 1:1:5) for 5 min. Both surfaces were thoroughly washed with distilled water, then dried under a gentle N_2 stream, and finally treated with UV/ozone for 10 min right before use.

After cleaning, the crystal was mounted inside the flow module. Distilled water was injected into the module one hour prior to the experiments for stabilization. The distilled water was then replaced with buffer or other sample solutions as specified in the main text. A baseline was established right before each test. Each test was repeated more than 5 times.

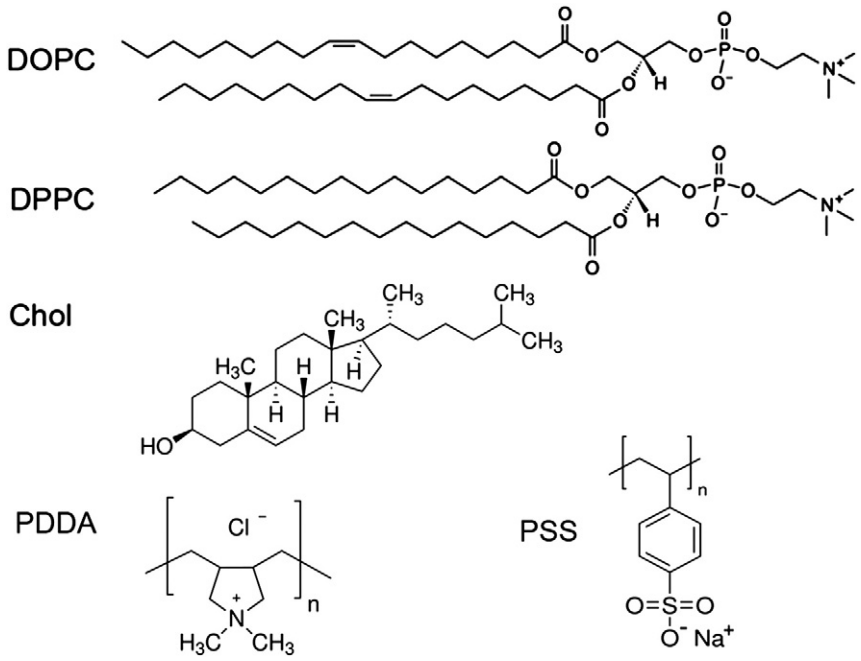

Fig. 1. Molecular structures of DOPC, DPPC, Chol, PDDA and PSS.

3. Interpretation of QCM-D measurements

Because of its extreme sensitivity to changes in mass and viscoelasticity of the loading onto the crystal sensor surface in real time and in situ, QCM-D has been regarded as an effective tool to investigate the dynamic processes at a solid/solution interface [13,33,34]. The parameters measured in a QCM-D experiment are the changes in oscillation frequency (Δf) and energy dissipation (ΔD) with time, at various harmonics (from 3rd to 13th in our experiments). When mass is adsorbed to the surface, the resonance frequency (f) decreases proportionally to the added mass, and vice versa. It is noted that the mass acquired includes both the mass of the materials and the water associated to the chip surface (probably the water hydrated by the materials). Parameter D represents the viscoelasticity of the layer on the surface. A high D indicates the layer on the surface is thick and soft, while a low D refers to something that is rigid and compact.

In addition to mass and viscoelasticity, the f and D values at different harmonics can provide three dimensional information of the layer on the surface, as the penetration depth of the harmonic wave is inversely proportional to its frequency. That is, a higher harmonic probe closer to the sensor surface than a lower harmonic [9,35]. Therefore, for a membrane related process, by analyzing the responses of f and D at different overtones during the dynamic interactions, the inherent structural information of the membrane, from the membrane surface to the whole membrane, can be acquired. In addition, the f and D data can be analyzed in a Δf versus ΔD plot. The Δf–ΔD plot consists of a number of discrete points and each point represents the values of Δf and ΔD at a certain time. They essentially show how the structure of the membrane changes with per unit mass addition. Furthermore, the distribution of the points correlates to the kinetics of the process. A sparse distribution indicates a rapid kinetics and vice versa. Finally, the Δf–ΔD trace highlights mechanistic processes. That is, where there is a change in the direction of the trace there is a different process occurring [32]. Particularly, it has been viewed as a fingerprint for the AMP–membrane interaction, which promises the possibility to help understand the underlying relationship between the amino acid residue activity and the peptide–membrane interaction mechanism [9,32].

4. Results and discussion

4.1. Surface coating characterization

The PDDA/PSS coating was deposited in situ before vesicle injection through electrostatic layer-by-layer assemblies of oppositely charged polyelectrolytes onto a SiO_2 surface of the sensor crystal. Fig. 2a shows the real-time QCM-D measurements, demonstrating the successive introduction of sample solutions as specified in the image. The injection of polyelectrolyte (PE) solutions (i.e. PDDA or PSS) induces a decrease in Δf and an increase in ΔD, until a constant value is reached, which obviously correspond to an overall increase in mass and energy dissipation on the sensor surface. Meanwhile, the responses measured at different overtones spread out obviously. When the PE solution was replaced with a buffer solution, the responses at different overtones overlapped instantaneously and show a much reduced magnitude (in absolute value).

The whole process can be further demonstrated in the Δf–ΔD plots. Here, the Δf values are plotted in reverse on the x-axis in order to reflect a mass increase (as $-\Delta f \cong \Delta m$), and ΔD values are plotted directly on the y-axis presenting the change of viscoelasticity of the probe. Then a north–south-east–west terminology can be used to interpret the Δf and ΔD (i.e. mass and viscoelasticity) changes during the dynamic process (Fig. 2b-inset). That is, for a dynamic process directing toward the east (i.e. increase in $-\Delta f$), mass is adding to the surface; conversely, if the process is pointing west, mass is losing. On the other hand, for a process pointing north (i.e. increase in ΔD) or south (decrease in ΔD), the layer on the surface is becoming more or less rigid, respectively [32]. In Fig. 2b, the incubation periods in PDDA and PSS solutions present as similar triangular patterns, which can be divided into two characteristic dynamic processes. The first process (labeled i) begins instantaneously after the injection of the PE solution. It is presented by a north-east arrow in the Δf–ΔD plots, corresponding to an increase in both mass and viscoelasticity on the surface. Furthermore, the responses at different overtones spread out greatly, indicating an uneven distribution of the adsorbed mass from the membrane surface to the whole membrane (*cf.* Section 3). This is characteristic for the deposition of a layer (PE molecules herein) on the surface [9,12,32]. Then, buffer injection induces a south-west process (ii) demonstrating a decrease in mass and viscoelasticity. It indicates that under buffer rinsing, the mass of the pre-adsorbed layer is somewhat lost and the film becomes rigid approaching the initial state before PE adsorption. This process suggests the rinsing away of much of the pre-adsorbed PE molecules, leaving only a thin and contact PE layer on the surface. Furthermore, the overlapping of Δf (and ΔD) at different overtones during this process indicates the homogeneity of the layer in the direction vertical to the surface. Besides these two processes, a third stage (iii) is also observed during the buffer rinsing process after the initial deposition of PDDA layer. It is presented by a net east arrow, which refers to a solely mass increase without much disturbance to the viscoelasticity of the layer. This process is possibly associated with the entire hydration of the charged polymer molecules within the

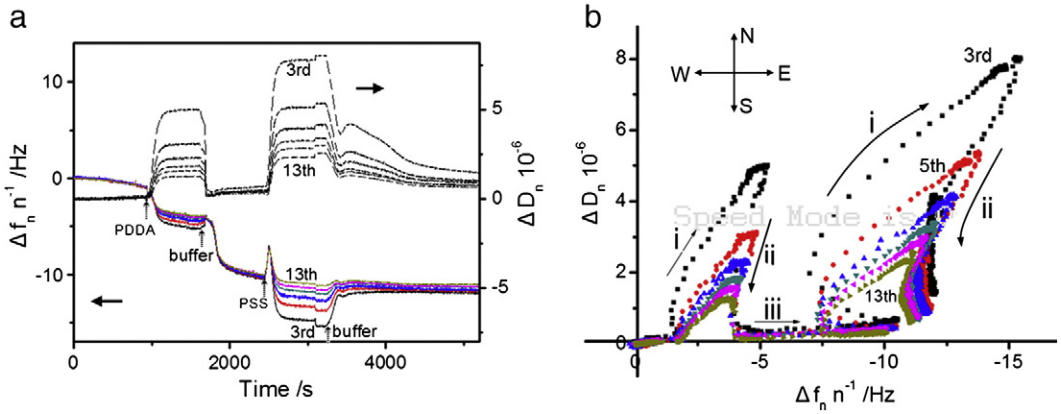

Fig. 2. Real-time QCM-D responses at different overtones (from 3rd to 13th), showing the successive deposition of PDDA and PSS on a SiO_2 surface of a sensor crystal. (a) Changes of Δf and ΔD with time on the introduction of certain solutions (marked with dotted arrows). (b) Corresponding Δf–ΔD plot. To assist understanding, arrows (labeled i–iii) are shown to represent different stages during the process. Inset, a north–south–east–west terminology used to interpret the Δf and ΔD changes during the dynamic process.

pre-adsorbed layer. Note that such process no longer exists after the deposition and binding of the oppositely charged PSS molecules. Another possibility is that more water molecules are diffused into and trapped between the bottom leaflet of the membrane and the sensor surface, increasing the overall mass measured without changing the energy dissipation [32]. (Upon the PSS injection, much of the coupled and/or trapped water was spelled out, shown as a reverse turning in the Δf–ΔD plots.) After the PDDA/PSS assembly, the value of Δf reached a steady state of -11.5 ± 0.5 Hz, and the frequency measured by all overtones was the same. Meanwhile, the value of ΔD (except the 3rd overtone) came back to a small value of $0.8 \pm 0.2 \times 10^{-6}$, indicating the formation of a close-packed coating layer. The larger magnitude of the 3rd overtone (~1.4×10^{-6}) may be due to the surficial swollen of the PE molecules in an aqueous solution.

4.2. Time-resolved vesicle deposition and deformation on different substrates

It has been generally accepted that the SLB formation from vesicles, at least in the case of zwitterionic lipid, includes the adsorption of vesicles on the substrate and the rupture of the adsorbed vesicles to form a confluent SLB, after a critical vesicle concentration is reached [12,24,36,37]. One of the key factors to determine the transformation from vesicle to SLB is the interactions between the adsorbed vesicles and the substrate surface. Therefore, the physicochemical properties of a substrate surface would greatly influence the deformation behavior of the vesicles adsorbed.

Dynamic vesicle deposition on different substrates, i.e., SiO_2, Au, and SiO_2/PDDA/PSS, was monitored by the time-resolved QCM-D measurements as shown in Fig. 3. From the time 0 s, vesicle solution was injected into the systems and kept flowing at a constant rate. For all the three systems, upon vesicle injection, the frequency responses decrease, and the dissipation responses increase, shown as a north-east arrow (labeled i) in the inset of the Δf–ΔD plots. This tendency indicates an increase in mass and viscoelasticity, referring to a distinct vesicle adsorption process. The measured responses at the end of this vesicle adsorption process (at the minimum Δf and maximum ΔD point for SiO_2) are characterized by a large dissipation, i.e. $\Delta D/\Delta f \sim 8.8 \pm 0.1 \times 10^{-8}$ for SiO_2 and $10.4 \pm 0.2 \times 10^{-8}$ for the Au and PE coated surfaces, and both the frequency and dissipation responses display obvious overtone dependencies (not shown here) that are characteristic of acoustically nonrigid films. These phenomena are consistent with the formation of an adsorbed vesicle layer [12]. On the other hand, it is noted that the initial decreases of Δf of the naked and PE-coated SiO_2 (i.e. SiO_2/PDDA/PSS surface) show a similar gradient, pronouncedly steeper than that of the Au surface. This means that the mass attraction in the former cases takes place much faster. The adsorption of vesicles is dictated to a large extent by the interplay between the surface chemistry of the vesicles and that of the solid support [37]. In contrast to Au, the electrostatic interaction, between the negatively charged substrate (SiO_2 and PSS) and the zwitterionic PC head groups within the vesicle membrane, is expected to facilitate the vesicle attraction process [38].

The interactions of the adsorbed vesicles with the substrate and adjacent vesicles predominantly determine whether vesicle rupture occurs [37]. On the bare SiO_2 surface, a characteristic dip/peak appears in the frequency/dissipation response, with time, which is shown as a reversing arrow (from north-east to south-west, labeled ii) in the Δf–ΔD plots, after passing a turning point. Furthermore, the final shifts in Δf (and ΔD) at different overtones overlapped (not shown here). These phenomena are characteristic of vesicle adsorption followed by SLB formation, after reaching a critical vesicle concentration [12]. The ultimate shifts in frequency ($\Delta f_{final} \sim -26 \pm 0.5$ Hz) and dissipation ($\Delta D_{final} \sim 0.5 \times 10^{-6}$) are approaching the characteristic values of those of a high-quality solid-supported bilayer, with a much reduced $\Delta D/\Delta f \sim 1.9 \pm 0.1 \times 10^{-8}$ [13]. On the other hand, for the other two substrates, no obvious vesicle rupture was observed. The frequency response keeps decreasing and dissipation response keeps increasing until saturation, indicating a monotonous adsorption process of vesicles on the surface. In addition to the surface chemistry of the substrate [38], a variety of factors including the lipid composition, the buffer pH and temperature, and the addition of divalent calcium cation, would also affect the dynamic vesicle deposition process [12,24].

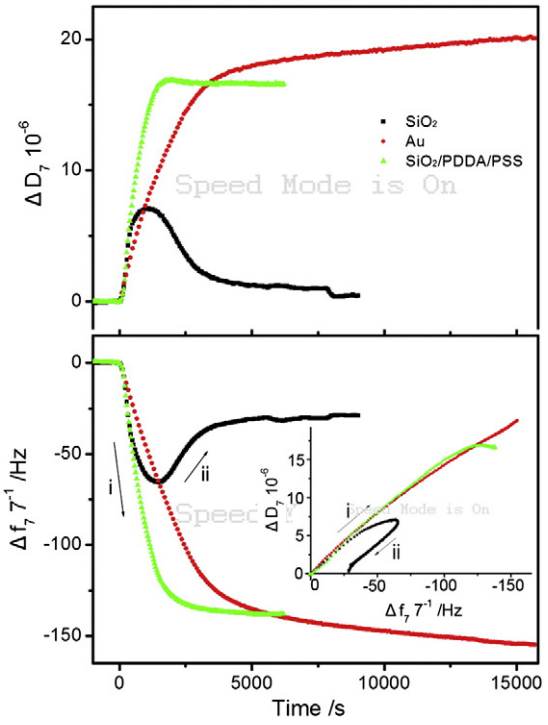

Fig. 3. QCM-D measurements showing the frequency (Δf) and dissipation (ΔD) responses upon deposition of lipid vesicles on different substrates: SiO_2, Au, and SiO_2/PDDA/PSS. The measurements are also plotted as Δf–ΔD curves in inset. The solid arrows labeled i and ii correspond to two different mechanistic processes during vesicle deposition. The 7th overtone is adopted and analyzed here.

4.3. Kinetics of interactions between melittin and a supported lipid bilayer (SLB)

The obtained SLB on a naked SiO_2 substrate was exposed to the solution of melittin, a kind of pore-forming peptide, to investigate the dynamic interactions between them. Fig. 4a shows the overtone effect under QCM-D measurements during the whole process of SLB formation (left part, labeled i and ii) and the following melittin–membrane interactions (right part, iii and iv). Upon the injection of melittin, an obvious decrease of Δf occurs immediately (iii), followed by an increase (iv), corresponding to the increase and decrease in ΔD respectively, until a steady state is reached. Furthermore, during the whole process, the values of Δf (or ΔD) measured by different overtones deviate dramatically from each other. After the interaction process, the frequency response reached a final value of -45 (to -35, from 3rd to 13th overtone) $\pm$ 0.5 Hz, and the dissipation response was 9 (to 3, respectively) $\pm 0.5 \times 10^{-6}$, being much larger (in absolute value) than those before the interaction occurred. In the Δf–ΔD plots in Fig. 4b, the initial decrease (increase) in Δf (ΔD) is shown as a north-east tendency (labeled iii) to a much increased dissipation with $\Delta D/\Delta f$ of about 20.1 (to 11.3, from 3rd to 13th overtone) $\times 10^{-8}$, and the following increase (decrease) in Δf (ΔD) presents as a reverse arrow (labeled iv) with a final $\Delta D/\Delta f$ of about 20.2 (to 7.9, from 3rd to 13th overtone) $\times 10^{-8}$, after reaching a turning point. This phenomenon is consistent with a "carpet" mechanism [24]. Here, process iii indicates an obvious increase in both mass and viscoelasticity (especially on the surface of the membrane as the lower harmonics show a greater

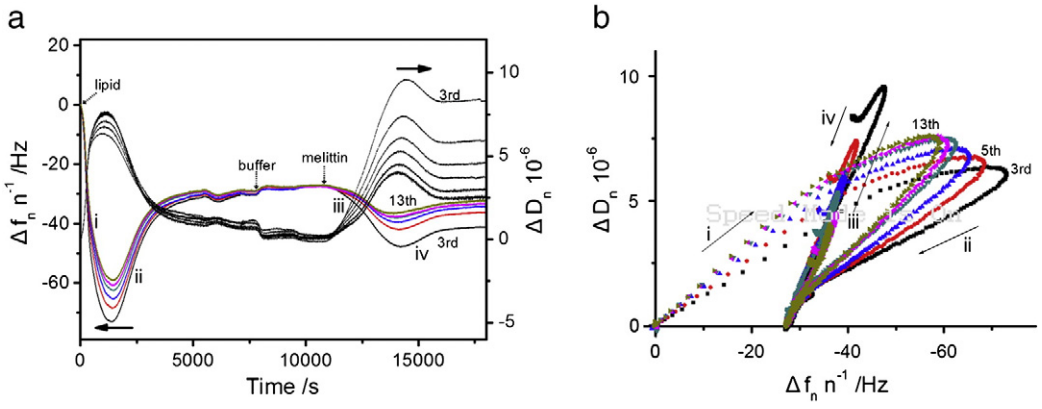

Fig. 4. (a) Real-time QCM-D responses, Δf and ΔD, at different overtones (from 3rd to 13th) during the vesicle deposition and membrane–melittin interaction processes on a naked SiO_2 substrate. Dotted arrows suggest the introduction of certain solutions. (b) Corresponding Δf–ΔD plots. Solid arrows labeled (i) to (iv) refers to four distinctly different processes during the whole measurement.

increase of mass and viscoelasticity), which probably refers to an adsorption of peptide molecules on the pre-formed membrane [32]. The adsorption is possibly accompanied by an arrangement of the peptide in the membrane, for example, penetration and diffusion in the lipid bilayer. Then, after reaching a threshold peptide concentration, process iv begins, with a demonstrated decrease in mass and energy dissipation (especially at the 13th overtone, i.e., of the whole membrane). This might correspond to the losing of part of the layer (probably the removal of some lipid–peptide complexes), and the decrease in dissipation (especially at the 13th overtone) indicates a significant rearrangement of the molecules over the whole membrane. It is noted that the slope of the curves during processes iii and iv at different overtones overlapped, in comparison to the spreading out traces during the vesicle deposition and rupture processes of i and ii. This indicates that upon per unit mass addition, the changes in viscoelastic property of the membrane, from the surface of to the whole layer, is the same. This excludes the possibility that the peptide only binds to the surface of the membrane and expels the swollen water from the membrane without lipid removal. Despite this, the f (and D) responses at different overtones deviated significantly from each other, indicating an asymmetrical structural transition of the layer throughout the membrane thickness.

4.4. Implication of melittin action upon vesicle matrix on an Au or PE coated surface

As a follow-up experiment, the interactions between melittin and the vesicle matrix deposited on other substrate surfaces, Au and SiO_2/PDDA/PSS, were studied. Under QCM-D monitoring, the interaction between melittin and a vesicle layer shows more complicated behavior than that with SLBs, which is ascribed to the coexistence of several interlinked and consecutive procedures: melittin association, insertion, rupture of vesicle, and final stabilization of the residual membrane.

Fig. 5 is the real-time QCM-D traces showing the full-range experimental process including the vesicle deposition and subsequent in situ vesicle–melittin interactions on an Au surface. Upon the injection of melittin, the system behaves in a much more complicated mode compared to that during the melittin–SLB interaction process (i.e. Fig. 4). However, a remarkable dip/peak in the frequency/dissipation responses (marked with */**) is obviously distinguishable, indicating the significant melittin adsorption process (i) followed by a stage dominated by mass removal (ii), after reaching a threshold peptide concentration. This is characteristic of a "carpet" mechanism, consistent with that for the melittin–SLB interaction (Fig. 4a). The mass removal here includes both the release of lipids, probably as lipid–melittin complex, and the leakage of vesicle components (mostly water molecules). This phenomenon was also observed during the interactions between melittin and vesicle matrix on the PE coated surface (*cf.* Figure S3).

Since the Voigt model is strictly valid for homogeneous viscoelastic films, the f and D parameters here may not represent absolute estimates of the film thickness and film viscosity, but served to qualitatively analyze the structural changes during the membrane–melittin interactions [39]. After the initial melittin adsorption process, fluctuation occurred in the f and D traces with time (ii to iv), demonstrating the arising of several competitive processes. However, after a long-time reaction of about 11 hours, the values of both Δf and ΔD came back gradually approaching 0. A final frequency response of -36 ± 5 Hz was obtained, being much smaller (in absolute value) than that before melittin injection (-160 ± 10 Hz). Meanwhile, the dissipation response went down from $19 \pm 2 \times 10^{-6}$ to $3.5 \pm 0.5 \times 10^{-6}$. Similar results were also obtained in the PE-coated system (*cf.* Figure S3). It is noted that for the contact vesicle layer before melittin injection, the dissipation of the film presents a much larger value on the 13th overtone compared to that on the 3rd one (Fig. 5c). The same distribution rule was also observed after melittin adsorption at the end of stage i ($\Delta D/\Delta f \sim 13.1$ to 20.0×10^{-8}, from 3rd to 13th overtone). This phenomenon further confirms the survival of the vesicles during this process. However, after the melittin action process, the dissipation displays a reverse overtone dependence that $\Delta D/\Delta f$ equals from 16.7 to 8.7×10^{-8}, from the 3rd to the 13th harmonic. These final values are comparable to the magnitude of those obtained from the melittin–SLB interactions on a bare SiO_2 surface, from which we can propose that after melittin exposure, the vesicle matrix disintegrates leaving only a layer of lipid membrane (probably with defects such as lipid–peptide complexes) behind, similar to that happened after melittin–SLB interactions. Comparison of the Δf–ΔD plots of QCM-D measurements on all the three substrates, i.e., naked SiO_2, Au and PE-coated surfaces, are shown in Fig. 6. It displays the whole process of vesicle deposition and subsequent melittin–membrane interactions. During the last stage of the melittin action process (arrow labeled "last"), the slope of the curve of Au or PE-coated system is nearly parallel to that of the bare SiO_2 substrate. As peptides with similar Δf–ΔD traces are reported to have similar mechanisms of action [32], the parallel distribution of Δf–ΔD plots here probably refers to a uniform membrane stabilization mechanistic process in all the three systems.

Furthermore, it is noted that the interaction of peptide with vesicle matrix takes a much longer (>40,000 s) time than with SLB (~5000 s). Besides the difference in the quantity of lipids in a SLB and a layer of contact vesicles, the difference in inherent mechanism is expected to be significant. To obtain more insights into the mechanisms underlying this melittin–membrane interaction process, computer simulation method was introduced.

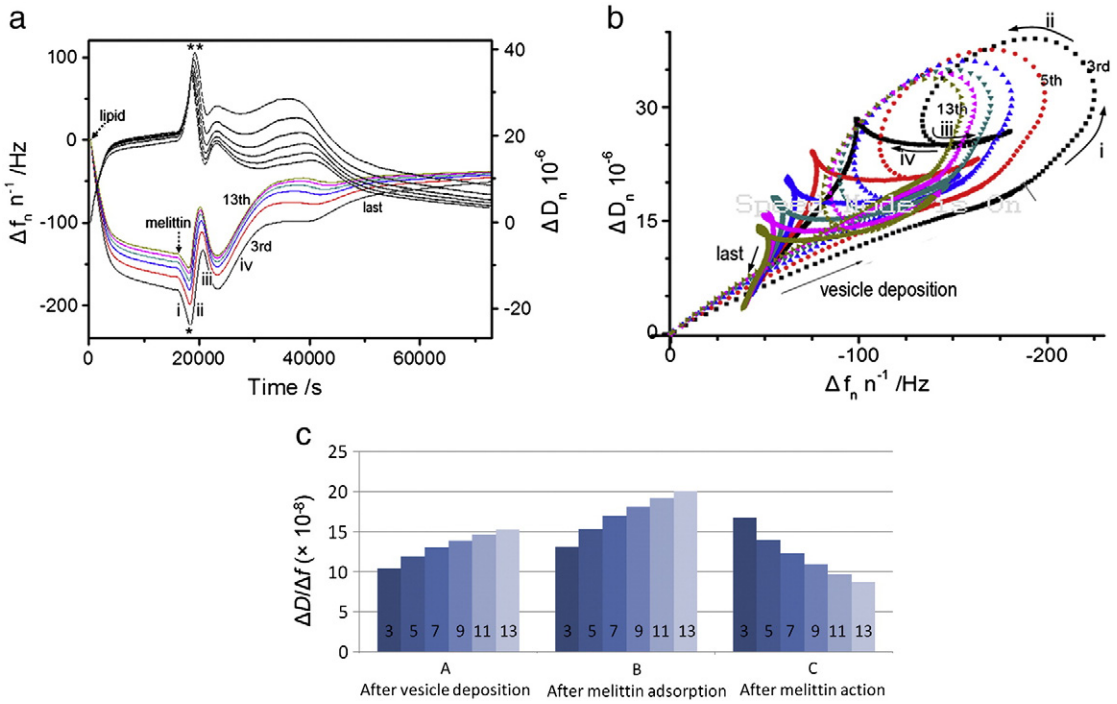

Fig. 5. (a) QCM-D traces at different overtones upon vesicle deposition and membrane–melittin interaction processes on an Au coated sensor surface. The dotted arrows refer to the introduction of certain solutions. (b) Corresponding Δ*f*–Δ*D* plot. To assist understanding, solid arrows were added representing the initial vesicle deposition and various stages (labeled i, ii, iii, iv, and last) during the subsequent membrane–melittin interactions. (c) Overtone effect on the Δ*D*/Δ*f* distributions at three model stages during the interaction process: A, after vesicle deposition, B, after melittin adsorption, and C, after melittin action.

4.5. Dissipative particle dynamics (DPD) simulations

DPD is a kind of coarse-grained computer simulation technique that has been extensively used to explore the interaction between lipid membrane and proteins [40–44]. In DPD simulations, each bead stands for a group of atoms or molecules. The evolution of the position and velocity of bead *i*, $\left(\vec{r}_i, \vec{v}_i\right)$, obeys Newton's equation of motion: $d\vec{r}_i/dt = \vec{v}_i, d\vec{v}_i/dt = \vec{f}_i/m$. The interaction between two beads is denoted as $\vec{F}_{ij}^{C} = a_{ij}(1 - r_{ij}/r_c)\vec{e}_{ij}$. Here, a_{ij} represents the maximum repulsion interaction between beads *i* and *j*, $\vec{r}_{ij} = \vec{r}_i - \vec{r}_j$, $r_{ij} = \left|\vec{r}_{ij}\right|$, and $\vec{e}_{ij} = \vec{r}_{ij}/r_{ij}$. Furthermore, random force and friction are applied to each pair of neighboring beads to keep the momentum locally conserved and to produce the hydrodynamic effect. The detailed settings of the parameters in simulation follows closely the method previously described (*cf.* Supporting Information) [40].

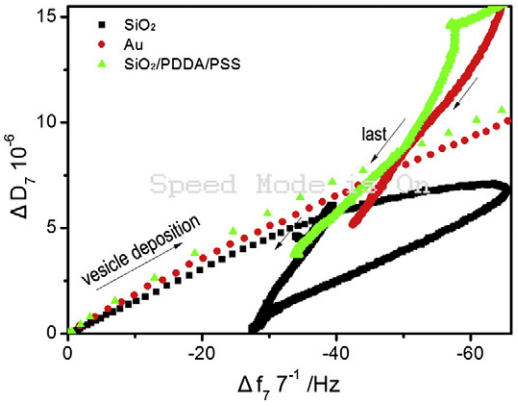

Fig. 6. Δ*f*–Δ*D* plots (partial view) of the QCM-D measurement upon vesicle deposition and subsequent melittin–membrane interaction processes on different substrates: SiO_2, Au, and SiO_2/PDDA/PSS. The slopes of the initial vesicle adsorption and the last stage of membrane disruption processes are emphasized with arrows. All the three measurements began at the right time of vesicle injection. The 7th overtone is adopted and analyzed here and the other overtones show similar rules.

During the peptide–membrane interactions, for a small peptide such as melittin, the most important difference between the membranes of a planar bilayer and a vesicle (about 110 nm in size) matrix is supposed to be the packing state of lipids. Here, the lipid packing state mainly describes the configuration of the lipid molecules, especially the lipid tails, in a bilayer [45]. It is quantified by the parameters such as the occupied area per lipid molecule (i.e. *APL*), and it provides information on the intermolecular interactions in a bilayer. In our simulations, membranes with different lipid packing states (and consequently with different surface tensions) were employed. A planar lipid bilayer with nearly zero surface tension is first produced for the SLB. A lipid-quantity-varied DPD method is applied to maintain the surface tension constant during the whole simulation process, regardless of the disturbance from milittin adsorption or insertion. In one of our previous work we mimicked the dynamic interaction process between melittin and lipid bilayer on molecular-level [24]. We found that for a lipid bilayer with zero surface tension, melittin can insert into the membrane (Figure S4) and the insertion capacity (i.e. the melittin inserted as a percentage of the total number of melittin under consideration in simulations) mainly depends on the local number-density of melittin on the bilayer surface, i.e., the local peptide-to-lipid ratio. With a melittin number-density from $n_p/area$ = 1/1024 to 9/81 (nm^2) (n_p denotes the total number of melittin under consideration; *area* stands for the area of the lipid bilayer), the insertion capacity of melittin increases from ~60% to almost 100% (Fig. 7, panel A) [24].

However, within a vesicle matrix system, the lipid packing state of the membrane becomes more complicated. Here, a system with a smaller lipid packing state, decreased from the equilibrium state of *APL* = 0.81 to 0.75 r_c^2 (r_c, the length unit in simulation, corresponding to ~0.8 nm) [40,41], is produced to roughly mimic the vesicle matrix system in the experiment. The dynamic insertion behaviors of melittin

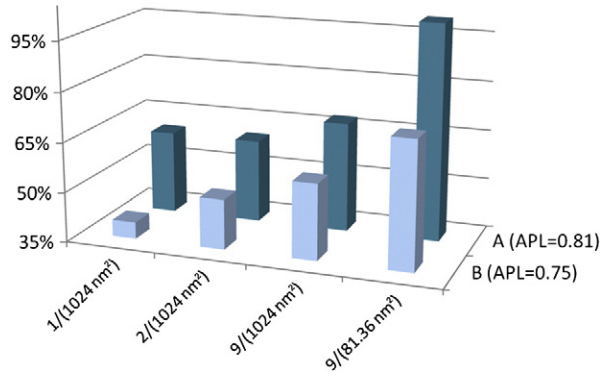

Fig. 7. Number-density dependence of the insertion capacity of melittin into membrane with different lipid packing states: A, *APL* = 0.81, stands for an equilibrated flat bilayer; B, *APL* = 0.75. All the results were obtained from an average of five independent simulations.

with different local peptide-to-lipid ratios were demonstrated as shown in Figure S5. It is found that under such a lipid packing state, the local morphology of the bilayer changes from a flat one to a curved one, and this transformation significantly influences the insertion custom of melittin. The insertion capacity of melittin shows decreases of about 25% (±5%) at various local number densities of melittin (Fig. 7, panel B). As the response behavior of lipids upon peptide adsorption was found to greatly influence their interactions [24], it is suggested here the lipid packing state within bilayer should be one of the significant factors influencing the molecular interaction between a peptide and the lipids.

5. Conclusions

In this work, QCM-D technique combined with computer simulations were employed to investigate on different substrates the deposition and deformation of vesicles, and the subsequent dynamic interactions between the fabricated membranes and melittin. High-quality SLB was formed on the naked SiO_2 surface while on an Au or polyelectrolyte coated substrate, a layer of intact vesicles was obtained. During the subsequent melittin exposure process, QCM-D monitoring showed that for both the SLB and vesicle matrix systems, similar "carpet" interaction manner and membrane stabilization effect were adopted. However, the morphology of the membrane significantly influenced the membrane-acting behavior of melittin, such as the acting efficiency and ability of melittin to insert into membrane. This effect is assumed to be closely associated with the lipid packing state of the membrane. Computer simulation was also employed to help understand the QCM-D results.

Acknowledgement

This work was financially supported by the National Science Foundation of China (Nos. 91027040, 31061160496, 21106114, and 11104192) and the National Basic Research Program of China (No. 2012CB821500). B.Y. thanks the Natural Science Foundation of Jiangsu Province of China (No. BK2012177). K.Y. thanks the support of the Key Project of Chinese Ministry of Education (No. 210208) and the Applied Basic Research Program (No. 2010CD091).

Supporting Information Available. DLS data; The detailed simulation method; QCM-D traces upon vesicle deposition and membrane–melittin interaction processes on the PE coated sensor surface; Snapshots of computer simulations during the melittin insertion process (n_p = 1 and 9) into membranes of various lipid packing states.

Appendix A. Supplementary data

Supplementary data to this article can be found online at http://dx.doi.org/10.1016/j.bbamem.2013.04.013.

References

[1] P. Mueller, D.O. Rudin, H.T. Tien, W.C. Wescott, Reconstitution of cell membrane structure in vitro and its transformation into an excitable system, Nature 194 (1962) 979-&.
[2] E. Sackmann, Supported membranes: scientific and practical applications, Science 271 (1996) 43–48.
[3] M. Tanaka, E. Sackmann, Polymer-supported membranes as models of the cell surface, Nature 437 (2005) 656–663.
[4] E. Reimhult, M. Zach, F. Hook, B. Kasemo, A multitechnique study of liposome adsorption on Au and lipid bilayer formation on SiO_2, Langmuir 22 (2006) 3313–3319.
[5] X.J. Han, A. Studer, H. Sehr, I. Geissbuhler, M. Di Berardino, F.K. Winkler, L.X. Tiefenauer, Nanopore arrays for stable and functional free-standing lipid bilayers, Adv. Mater. 19 (2007) 4466–4470.
[6] X.J. Zhou, J.M. Moran-Mirabal, H.G. Craighead, P.L. McEuen, Supported lipid bilayer/carbon nanotube hybrids, Nat. Nanotechnol. 2 (2007) 185–190.
[7] P.K. Ang, K.P. Loh, T. Wohland, M. Nesladek, E. Van Hove, Supported lipid bilayer on nanocrystalline diamond: dual optical and field-effect sensor for membrane disruption, Adv. Funct. Mater. 19 (2009) 109–116.
[8] C. Steinem, H.J. Galla, A. Janshoff, Interaction of melittin with solid supported membranes, Phys. Chem. Chem. Phys. 2 (2000) 4580–4585.
[9] A. Mechler, S. Praporski, K. Atmuri, M. Boland, F. Separovic, L.L. Martin, Specific and selective peptide–membrane interactions revealed using quartz crystal microbalance, Biophys. J. 93 (2007) 3907–3916.
[10] T. Shahal, K.A. Melzak, C.R. Lowe, E. Gizeli, Poly(dimethylsiloxane)-coated sensor devices for the formation of supported lipid bilayers and the subsequent study of membrane interactons, Langmuir 24 (2008) 11268–11275.
[11] K. Sugihara, J. Voros, T. Zambelli, A gigaseal obtained with a self-assembled long-lifetime lipid bilayer on a single polyelectrolyte multilayer-filled nanopore, ACS Nano 4 (2010) 5047–5054.
[12] N.-J. Cho, C.W. Frank, B. Kasemo, F. Hook, Quartz crystal microbalance with dissipation monitoring of supported lipid bilayers on various substrates, Nat. Protoc. 5 (2010) 1096–1106.
[13] Y.C. Tang, Z.N. Wang, J.W. Xiao, S.H. Yang, Y.J. Wang, P.E. Tong, Studies of phospholipid vesicle deposition/transformation on a polymer surface by dissipative quartz crystal microbalance and atomic force microscopy, J. Phys. Chem. B 113 (2009) 14925–14933.
[14] K.A. Brogden, Antimicrobial peptides: pore formers or metabolic inhibitors in bacteria? Nat. Rev. Microbiol. 3 (2005) 238–250.
[15] A.A. Stromstedt, L. Ringstad, A. Schmidtchen, M. Malmsten, Interaction between amphiphilic peptides and phospholipid membranes, Curr. Opin. Colloid Interface Sci. 15 (2010) 467–478.
[16] G.E. Fantner, R.J. Barbero, D.S. Gray, A.M. Belcher, Kinetics of antimicrobial peptide activity measured on individual bacterial cells using high-speed atomic force microscopy, Nat. Nanotechnol. 5 (2010) 280–285.
[17] A.C. Rapson, M.A. Hossain, J.D. Wade, E.C. Nice, T.A. Smith, A.H.A. Clayton, M.L. Gee, Structural dynamics of a lytic peptide interacting with a supported lipid bilayer, Biophys. J. 100 (2011) 1353–1361.
[18] M. Gordon-Grossman, Y. Gofman, H. Zimmermann, V. Frydman, Y. Shai, N. Ben-Tal, D. Goldfarb, A combined pulse EPR and monte carlo simulation study provides molecular insight on peptide–membrane interactions, J. Phys. Chem. B 113 (2009) 12687–12695.
[19] H. Raghuraman, A. Chattopadhyay, Melittin: a membrane-active peptide with diverse functions, Biosci. Rep. 27 (2007) 189–223.
[20] S. Joshi, G.S. Bisht, D.S. Rawat, A. Kumar, R. Kumar, S. Maiti, S. Pasha, Interaction studies of novel cell selective antimicrobial peptides with model membranes and *E. coli* ATCC 11775, Biochim. Biophys. Acta Biomembr. 1798 (2010) 1864–1875.
[21] S. Stankowski, M. Pawlak, E. Kaisheva, C.H. Robert, G. Schwarz, A combined study of aggregation, membrane affinity and pore activity of natural and modified melittin, Biochim. Biophys. Acta 1069 (1991) 77–86.
[22] L. Becucci, R.R. Leon, M.R. Moncelli, P. Rovero, R. Guidelli, Electrochemical investigation of melittin reconstituted into a mercury-supported lipid bilayer, Langmuir 22 (2006) 6644–6650.
[23] M. Gheorghiu, A. Olaru, A. Tar, C. Polonschii, E. Gheorghiu, Sensing based on assessment of non-monotonous effect detemined by target analyte: case study on pore-forming compounds, Biosens. Bioelectron. 24 (2009) 3517–3523.
[24] N.Y. Lu, K. Yang, B. Yuan, Y.Q. Ma, Molecular response and cooperative behavior during the interactions of melittin with a membrane: dissipative quartz crystal microbalance experiments and simulations, J. Phys. Chem. B 116 (2012) 9432–9438.
[25] H.W. Huang, Action of antimicrobial peptides: two-state model, Biochemistry 39 (2000) 8347–8352.
[26] A. Olaru, M. Gheorghiu, S. David, T. Wohland, E. Gheorghiu, Assessment of the multiphase interaction between a membrane disrupting peptide and a lipid membrane, J. Phys. Chem. B 113 (2009) 14369–14380.
[27] J.F. Popplewell, M.J. Swann, N.J. Freeman, C. McDonnell, R.C. Ford, Quantifying the effects of melittin on liposomes, Biochim. Biophys. Acta Biomembr. 1768 (2007) 13–20.
[28] H. Raghuraman, A. Chattopadhyay, Orientation and dynamics of melittin in membranes of varying composition utilizing NBD fluorescence, Biophys. J. 92 (2007) 1271–1283.

[29] H. Raghuraman, A. Chattopadhyay, Interaction of melittin with membrane cholesterol: a fluorescence approach, Biophys. J. 87 (2004) 2419–2432.
[30] P. Wessman, A.A. Stromstedt, M. Malmsten, K. Edwards, Melittin–lipid bilayer interactions and the role of cholesterol, Biophys. J. 95 (2008) 4324–4336.
[31] A. Lundquist, P. Wessman, A.R. Rennie, K. Edwards, Melittin–lipid interaction: a comparative study using liposomes, micelles and bilayer disks, Biochim. Biophys. Acta Biomembr. 1778 (2008) 2210–2216.
[32] G.A. McCubbin, S. Praporski, S. Piantavigna, D. Knappe, R. Hoffmann, J.H. Bowie, F. Separovic, L.L. Martin, QCM-D fingerprinting of membrane-active peptides, Eur. Biophys. J. 40 (2011) 437–446.
[33] B. Seantier, C. Breffa, O. Felix, G. Decher, Dissipation-enhanced quartz crystal microbalance studies on the experimental parameters controlling the formation of supported lipid bilayers, J. Phys. Chem. B 109 (2005) 21755–21765.
[34] B. Yuan, T. Zhu, Z.X. Zhang, Z.Y. Jiang, Y.Q. Ma, Self-assembly of multilayered functional films based on graphene oxide sheets for controlled release, J. Mater. Chem. 21 (2011) 3471–3476.
[35] F. Hook, B. Kasemo, T. Nylander, C. Fant, K. Sott, H. Elwing, Variations in coupled water, viscoelastic properties, and film thickness of a Mefp-1 protein film during adsorption and cross-linking: a quartz crystal microbalance with dissipation monitoring, ellipsometry, and surface plasmon resonance study, Anal. Chem. 73 (2001) 5796–5804.
[36] C.A. Keller, B. Kasemo, Surface specific kinetics of lipid vesicle adsorption measured with a quartz crystal microbalance, Biophys. J. 75 (1998) 1397–1402.
[37] M. Sundh, S. Svedhem, D.S. Sutherland, Influence of phase separating lipids on supported lipid bilayer formation at SiO_2 surfaces, Phys. Chem. Chem. Phys. 12 (2010) 453–460.
[38] C.I. Cheng, Y.-P. Chang, Y.-H. Chu, Biomolecular interactions and tools for their recognition: focus on the quartz crystal microbalance and its diverse surface chemistries and applications, Chem. Soc. Rev. 41 (2012) 1947–1971.
[39] G. Ohlsson, A. Tigerstrom, Fredrik Hook, B. Kasemo, Phase transitions in adsorbed lipid vesicles measured using a quartz crystal microbalance with dissipation monitoring, Soft Matter 7 (2011) 10749–10755.
[40] K. Yang, Y.Q. Ma, Computer simulation of the translocation of nanoparticles with different shapes across a lipid bilayer, Nat. Nanotechnol. 5 (2010) 579–583.
[41] K. Yang, B. Yuan, Y.Q. Ma, Curvature changes of bilayer membranes studied by computer simulations, J. Phys. Chem. B 116 (2012) 7196–7202.
[42] M. Venturoli, B. Smit, M.M. Sperotto, Simulation studies of protein-induced bilayer deformations, and lipid-induced protein tilting, on a mesoscopic model for lipid bilayers with embedded proteins, Biophys. J. 88 (2005) 1778–1798.
[43] U. Schmidt, G. Guigas, M. Weiss, Cluster formation of transmembrane proteins due to hydrophobic mismatching, Phys. Rev. Lett. 101 (2008) 128104.
[44] F.J.-M. de Meyer, J.M. Rodgers, T.F. Willems, B. Smit, Molecular simulation of the effect of cholesterol on lipid-mediated protein-protein interactions, Biophys. J. 99 (2010) 3629–3638.
[45] A. Ben-Shaul, Molecular theory of chain packing, elasticity and lipid protein interaction in lipid bilayers, in: R. Lipowsky, E. Sackmann (Eds.), Structure and Dynamics of Membranes, Elsevier, Amsterdam, 1995, pp. 359–402.